



# Ensemble-based virtual screening reveals dual-inhibitors for the p53–MDM2/MDMX interactions

Khaled Barakat<sup>a</sup>, Jonathan Mane<sup>b</sup>, Douglas Friesen<sup>b</sup>, Jack Tuszynski<sup>a,b,\*</sup>

<sup>a</sup> Department of Physics, University of Alberta, Edmonton, AB, Canada

<sup>b</sup> Department of Oncology, University of Alberta, Edmonton, AB, Canada

## ARTICLE INFO

### Article history:

Received 22 October 2009

Received in revised form 4 December 2009

Accepted 8 December 2009

Available online 14 December 2009

### Keywords:

p53

MDM2

MDMX

Virtual screening

Clustering

NCI database

DrugBank

Dual-inhibitor

## ABSTRACT

The p53 protein, a guardian of the genome, is inactivated by mutations or deletions in approximately half of human tumors. While in the rest of human tumors, p53 is expressed in wild-type form, yet it is inhibited by over-expression of its cellular regulators MDM2 and MDMX proteins. Although the p53-binding sites within the MDMX and MDM2 proteins are closely related, known MDM2 small-molecule inhibitors have been shown experimentally not to bind to its homolog, MDMX. As a result, the activity of these inhibitors including Nutlin3 is compromised in tumor cells over-expressing MDMX, preventing these compounds from fully activating the p53 protein. Here, we applied the relaxed complex scheme (RCS) to allow for the full receptor flexibility in screening for dual-inhibitors that can mutually antagonize the two p53-regulator proteins. First, we filtered the NCI diversity set, DrugBank compounds and a derivative library for MDM2-inhibitors against 28 dominant MDM2-conformations. Then, we screened the MDM2 top hits against the binding site of p53 within the MDMX target. Results described herein identify a set of compounds that have been computationally predicted to ultimately activate the p53 pathway in tumor cells retaining the wild-type protein.

Crown Copyright © 2009 Published by Elsevier Inc. All rights reserved.

## 1. Introduction

Tumor suppressor protein p53 is a key regulator of cell cycle, apoptosis, DNA repair and senescence [1–4]. In these processes, p53 responds to cellular stress, such as hypoxia and DNA damage, by accumulating in the nucleus and activating various pathways to maintain the cell's functional normality [5]. Because of its vital role as a guardian of the genome, tumor cells have developed numerous ways to disable its function. Indeed, the *Tp53* gene is mutated or deleted in ~50% of human cancers [6]. In the rest of human cancers, although p53 retains its wild-type form, the p53 activity is eradicated by its main cellular inhibitor, murine double minute 2 protein (MDM2) [7,8].

MDM2 is the main regulator for p53. In fact, MDM2 and p53 regulate each other through a feedback loop [7]. In this mechanism, p53 transcribes for MDM2, while MDM2 acts as an E3 ubiquitin ligase that exports p53 out of the nucleus and promotes its degradation. Moreover, by binding to the transactivation domain of p53 within the nucleus, MDM2 inhibits p53 function as a transcription factor for other proteins. Consequently, MDM2 is envisaged as an effectual inhibitor for p53. Certainly, over-

expression of MDM2 reduces the cellular ability to activate the p53 pathway under stress conditions. This abnormality of p53 regulation was initially discovered in sarcomas retaining wild-type p53, and it was later observed in several cancers as a common mechanism to disable p53 activity [9–11].

Structurally related to MDM2, MDMX (also known as MDM4) is a second cellular regulator of p53 [12]. Although MDMX lacks the intrinsic E3 ligase activity of MDM2 [13], current models suggest that it functions as a major p53 transcriptional antagonist independent of MDM2 [14]. The two proteins form a heterodimeric complex through their C-terminal RING domain interaction which, in turn, increases the ability of MDM2 to promote p53 degradation [15]. In fact, the MDMX–MDM2 interaction can also lead to ubiquitination and degradation of MDMX leading to the elimination of MDMX during DNA damage response [16]. The binding domains of p53 within MDM2 and MDMX are very similar (~80% sequence homology) [17], offering promise for the discovery of new small-molecule compounds that can target the two proteins simultaneously.

Recent studies proved that activation of the p53 pathway through a disruption of its interaction with MDM2 is a promising therapeutic strategy for cancers that retain the wild-type p53 [18–21]. In particular, the last decade has witnessed the identification of an increasing number of non-peptide, small-molecule MDM2-inhibitors with promising binding affinities [21]. These are analogs of *cis*-imidazoline (Nutlins) [22], spiro-oxindole (MI-63 and MI-

\* Corresponding author at: Department of Physics, University of Alberta, Edmonton, AB, Canada.

E-mail address: [jtus@phys.ualberta.ca](mailto:jtus@phys.ualberta.ca) (J. Tuszynski).

219) [23–26], benzodiazepinedione (TDP665759) [27–29], terphenyl [30], quinalin [31], chalcone [32] and sulfonamide [33]. Of these molecules only three compounds, namely, Nutlin3, MI-219 and TDP665759 showed sufficiently high binding affinity, and desirable pharmacokinetic profiles in cells [18]. However, these compounds are more highly selective for MDM2 than for its homolog MDMX. In particular, MI-219 showed a greater than 10,000-fold selectivity for MDM2 relative to MDMX [18] which is undesirable since p53 activation by Nutlin3 is compromised in cells over-expressing MDMX [34]. These results suggest that development of novel compounds that are MDMX-specific or optimized for dual-inhibition of MDM2 and MDMX is a necessary step to achieve full activation of p53 in tumor cells. Recently, Pazgier et al. [35] reported the development of a potent peptide inhibitor, termed PMI (p53–MDM2/MDMX-inhibitor) that can target the interactions of p53 with both MDM2 and MDMX. This peptide inhibitor provides the proof of concept for this strategy and opens the door for the discovery of novel small-molecule inhibitors that can mimic its function.

Receptor-based virtual screening (VS) is a well-established technique to uncover novel molecular inhibitors that complement a target protein in terms of shape, charge and several additional biophysical or biochemical properties [36]. Although VS applied against a crystal or relaxed receptor structure is a commonly used approach in structure-based drug design, the dynamic changes due to receptor flexibility are always neglected to the detriment of the predictive success of these methods. For instance, a ligand can induce significant conformational changes to its target, ranging from local reorganization of side-chains to hinge movement of domains [37]. Sampling these conformational changes during docking is impractical, as they involve too large a number of degrees of freedom.

One successful approach that has been reported by Bowman et al. in designing novel inhibitors for MDM2, is to build a dynamic receptor-based pharmacophore by probing conserved interaction spots in an ensemble of bound target structures [38]. Another technique to account for receptor flexibility is the relaxed complex scheme (RCS). In this method, molecular dynamics (MD) simulations are applied to explore the conformational space of the protein receptor, while docking is subsequently used for the fast screening of drug libraries against an ensemble of receptor conformations. This methodology has been successfully applied to a number of cases [39,40]. An excellent example is an HIV inhibitor, raltegravir [40], which became the first FDA-approved drug targeting HIV integrase. MD simulations played a significant role in discovering a novel binding site, and compounds that can exchange between the two binding sites have formed a new generation of HIV integrase inhibitors.

Here, we build upon these achievements and apply the RCS technique to account for the full receptor flexibility in screening for MDM2/MDMX dual-inhibitors. Our approach involved two major steps. First, we filtered a compound library of 6617 small molecules for novel MDM2-inhibitors. This library was comprised of the National Cancer Institute (NCI) diversity set, DrugBank small molecules and a set of ~3000 derivative structures based on Nutlin3a, MI-219 and TDP665759. It should be mentioned that, although MDM2 has been co-crystallized with Nutlin2 (PDB entry 1RV1) [41], the binding affinity of Nutlin2 is very low compared to Nutlin3a, compelling us to use Nutlin3a as a positive control in this study. The full set of compounds has been screened against an ensemble of MDM2 structures. The ensemble incorporated the MDM2 crystal structure in addition to the 27 principal conformations extracted from MD simulations. Finally, the top 300 hits that resulted from this screening exercise were filtered for compounds that can bind to MDMX with a sufficiently high affinity. The ranking of compounds involved two successive iterations. First, we

used AUTODOCK version 4.0 [42] to place the compounds within the binding sites of MDM2 and MDMX proteins and to search for their minimal energy conformations. Then, the irredundant top 300 hits from AUTODOCK screening were rescored using the molecular mechanics Poisson–Boltzmann surface area (MM–PBSA) method [43]. It is hoped that our results will eventually be used in the design of more potent and particularly specific inhibitors of the MDM2/MDMX–p53 interactions suitable for pre-clinical and clinical development.

## 2. Results and discussion

MDM2 is the major cellular inhibitor of p53 and its gene is significantly amplified in ~50% of cancers that retain wild-type p53 [7,8]. Consequently, targeting the p53–MDM2 protein–protein interaction has been a promising but very challenging cancer therapeutic approach for the last couple of years [18,19]. Genetic and biochemical studies limited the interaction between the two proteins to the 106-N-terminal domain of MDM2 and the N-terminus of the transactivation domain of p53. These studies have been based on a high-resolution crystal structure that demonstrates the essential interacting regions located in the MDM2–p53 interface. Essentially, p53 forms an amphipathic  $\alpha$ -helix peptide (residues 15–29) that is partly buried inside a small but deep, hydrophobic groove on the surface of the MDM2 N-terminal domain (residues 19–102). This interaction involves four key residues from p53, namely F19, L22, W23 and L26 and at least 13 residues from MDM2 (L54, L57, I61, M62, Y67, Q72, V75, F86, F91, V93, I99, Y100 and I103) [65,66]. Thus, a small-molecule inhibitor that mimics the p53-hot spot residues would ultimately disrupt this interaction and is assumed to completely re-activate the p53 pathway and restore the cell's functional normality. Unexpectedly, recent studies revealed that targeting the p53–MDM2 interaction is not sufficient to restore p53 activity, as there are other regulators that have been recently discovered and may play significant roles in controlling the p53 pathway. Of these regulators, MDMX, which is a protein that shares structural homology with MDM2, has been identified as an inhibitor for p53 [67]. Intriguingly, 10 out of the 13 most important MDM2 residues described above are conserved in MDMX, which indicates that the binding site of p53 within the surface of MDMX is similar to, but not identical with, that of MDM2. Based on these findings, it was assumed that inhibitors that target the MDM2–p53 interaction should function in the same way to disrupt the MDMX–p53 binding. Surprisingly, this was not the case, as most of MDM2-inhibitors, including Nutlin3 have been shown to be inactive in cancer cells over-expressing MDMX, opening a new avenue in p53 research and requiring a new generation of MDM2-inhibitors that can target its homolog, MDMX, as well.

To this end, most of the current efforts have been exclusively focused on uncovering small-molecule MDM2-inhibitors and little work has been done on targeting MDMX. These efforts incorporate computational three-dimensional database screening of large chemical libraries [33,31,38], experimental screening of chemical libraries [68,32,22,28], and structure-based de novo design [23,25]. Although the flexibility of the p53-binding site within the MDM2 target has been shown to be important [24], most of the non-peptide, small-molecule MDM2-inhibitors discovered computationally targeted a single rigid conformation extracted from the MDM2–p53 crystal structure. Conversely, Bowman et al. carried out the first study that incorporated receptor flexibility in designing a dynamic receptor-based pharmacophore model of MDM2 [38]. In designing this model Bowman et al. employed a multiple protein structures (MPSS) technique that probes conserved interaction regions within the MDM2-pocket. A conserved interaction was defined as the one that is present in most of the

protein conformations despite the intrinsic motion of the active site. The MDM2 structures have been extracted from a 2 ns MD simulation on the holo-protein. This strategy has led to the identification of five novel scaffolds, which inhibit the MDM2–p53 interaction.

Here, we have built on the success of these earlier pioneering efforts by screening the NCI diversity set (1883 compounds), the DrugBank set of small-molecules (1566 compounds) and more than 3168 derivative structures extracted from the known MDM2-inhibitors against 28 different MDM2 models that represent the apo- and holo-structure's collective conformational dynamics. The top 300 hits that showed strong affinity for MDM2 have been used in a second round of screening against the p53-binding site within MDMX. Results described herein represent the identification of dual-inhibitors that can disrupt the MDM2/MDMX–p53 interaction and allow for the full activation of the p53 pathway. Our primary use of docking techniques has been to filter the three medicinal chemistry compound libraries through receptor-based virtual screening, in an attempt to uncover molecules that complement the MDM2/MDMX binding sites in terms of such parameters as shape, charge, and several additional biochemical characteristics.

### 2.1. Molecular dynamics simulations of MDM2–p53 and PMI–MDMX interactions

To generate an ensemble of equilibrated MDM2 models for chemical library screenings, the N-terminal domain of MDM2 was subjected to MD simulations, in both its free and p53-bound states. The proper equilibration of these systems was essential in order to perform virtual screening on a set of rigid receptor models that represent, approximately the whole conformational space of the p53-binding site within MDM2. Furthermore, it is generally required to start with adequately sampled, energetically minimized models in order to eliminate unfavorable atom contacts that may have been introduced as a result of crystal packing in the original structure. We also used MD simulations to generate an equilibrated model for the PMI–peptide/MDMX complex introduced by Pazgier et al. [35] to filter the top hits from the MDM2 screening for those compounds that can mimic the characteristics of this peptide inhibitor. It should be noted that, as we used docking as a preliminary filtering step in screening the full set of compounds for MDM2-inhibitors, it was essential to generate an ensemble of MDM2 structures in order to partly incorporate protein flexibility during docking. In this context, we selected the top 300 compounds that can bind to their appropriate MDM2 conformation for post-docking analysis using MD simulations to introduce the full flexibility for both the ligand and its selected target structure. On the other hand, we did not generate such ensemble of structures for the MDMX-screening exercise because of the following reasons; First, docking runs were not used to filter the compounds for best binders, they were used to place each ligand from the 300 MDM2 top hits within the MDMX pocket and assemble a minimum energy protein–ligand conformation required for MD simulations. Second, the full flexibility of this complex will be established using a fairly long MD simulation (2 ns) that can reasonably explore the conformational space of the protein–ligand complex and simulate their induced fit interaction.

### 2.2. Principal Component Analysis and completeness of sampling

As MD simulations produce numerous conformations of the MDM2 and p53 proteins, we have utilized Principal Component Analysis (PCA) to transform the original space of correlated variables into a reduced set of independent variables comprising the essential dynamics of the system [54,55]. To perform PCA, the

entire MD trajectory must first be RMSD (root-mean-square-deviation) fitted to a reference structure and a covariance matrix is calculated from its Cartesian co-ordinates. The resulting eigenvectors constitute the essential vectors of the motion, where the larger an eigenvalue, the more important its corresponding eigenvector in the collective motion. PCA was performed over the entire MD simulations of both the holo- and apo-MDM2 structures using atoms comprising the 18 residues contained in the MDM2 binding site (residues numbered: 25, 26, 50, 51, 54, 58, 61, 62, 67, 72, 73, 93, 94, 96, 97, 99, 100, 104) with the backbone atoms RMSD fitted to the minimized crystal structure of the two starting configurations. We defined the binding site as comprised of the MDM2 residues that are located within 10 Å from p53-atoms. Resulting eigenvectors were sorted by descending eigenvalues, which represent the variance of the motion along the principal components. The ten dominant eigenvalues for the two simulated systems are shown in Fig. 1a. The first eigenvalue has a magnitude that is significantly higher than those of the other eigenvalues. The components with the largest eigenvalues represent correlated motions of the binding site with the most significant standard deviations of the motion along the corresponding orthogonal directions.

Fig. 1b represents the spatial distributions of occupancies for the conformational states over the planes spanned by the three dominant principal components of the binding site for the two systems. The p53-binding site within MDM2 adopted several conformations throughout the MD simulations, indicating the flexibility of the protein. The grouping of MD trajectories into a limited number of clusters suggests the presence of favored folded conformations and significant basins of attraction.

Covariant analysis of the trajectories from the holo- and apo-MD simulations, successively divided into thirds, was performed using the same procedure used for PCA. Normalized overlaps calculated between each of these thirds are reported in Table 1. The high overlap between the thirds indicates that each part of the simulation samples approximately the same conformational space, and it is unlikely that there are unexplored regions missed earlier in the runs. Although there is no guarantee that complete equilibrium sampling is given, we have concluded that the observed overlap is acceptable and adequate sampling within the MD trajectories for the binding site had been obtained.

Plots of the RMSDs for the backbone atoms from the initial co-ordinates of the p53 peptide and MDM2, both free and bound to p53, for the last 10 ns of the simulation illustrate the inherent stability of the complex (see Fig. 2). For the apo-MDM2 simulations, the protein backbone RMSD fluctuated about a mean of 1.9 Å. On the other hand, the holo-system fluctuated around lower RMSD values for both MDM2 and the p53 peptide of 1.3 and 1.5 Å, respectively, indicating a mutually stabilizing effect induced by protein–protein interactions. This observation was also confirmed by results presented in Fig. 3a, where the apo-MDM2 main-chain B-factors (averaged over heavy atoms) for the residues constructing the p53-binding site within MDM2 (residues 68–73, 85–102 and 104–105) are higher than the corresponding holo-MDM2 values. This suggests the relative flexibility of the

**Table 1**

PCA normalized overlap for the p53-binding site within MDM2. Covariance analysis has been performed for the three thirds of the MD trajectories for the apo (free) and holo (bound) systems followed by calculating the overlap between their covariance matrices.

apo-MDM2	holo-MDM2	
0.761	0.754	1st and 2nd
0.732	0.811	1st and 3rd
0.734	0.792	2nd and 3rd

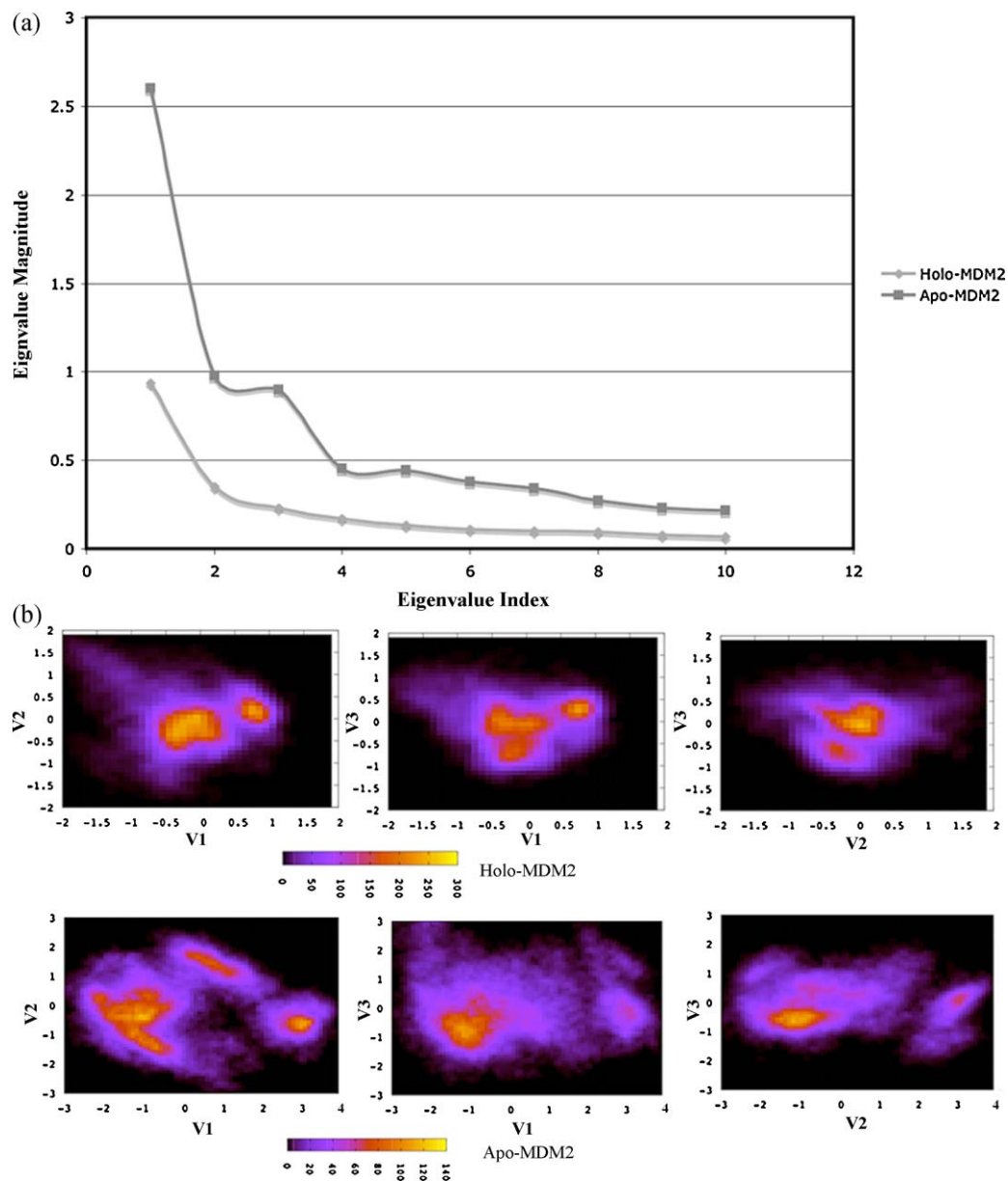


**Fig. 1.** PCA for the MDM2 binding site. (a) The dominant ten eigenvalues for the apo and holo trajectories. (b) Projections of the ensemble of conformations onto the planes of the three most important principal components. The first and second, the first and third and the second and third principal components are plotted on the x and y axes, respectively, for the two systems. The histograms represent the occupancies of the corresponding conformation states, with lighter colors indicating more frequently visited areas.

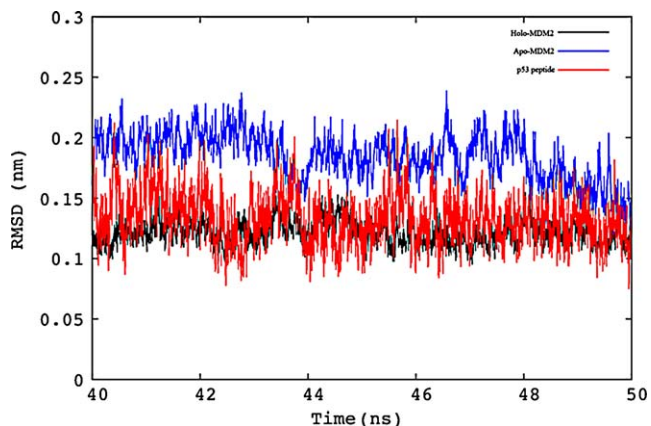


**Fig. 2.** Plot of the RMSD of the backbone atoms from the reference structure as a function of simulation time in p53-peptide, MDM2-free and MDM-p53 complex.

model in this region where the 18 residues defining the binding site seem to be relatively rigid during the MD simulation in the p53-MDM2 models. On the p53 side, residues 19–26 (see Fig. 2b) are more rigid than other p53 residues, suggesting their critical participation in binding to MDM2.

### 2.3. Ensemble-based virtual screening

While integrating receptor flexibility into docking reduces the risk of unfavorable ligand–target interactions, accommodating full receptor flexibility during a docking experiment is impractical [27]. One solution for this problem is to allow only those parts of the receptor that affect the protein–ligand interactions to be flexible during docking. Due to the increased sampling requirements and limited computational resources, flexible parts are generally restricted to the principal side chains that are believed to be involved in binding interactions. This procedure allows for



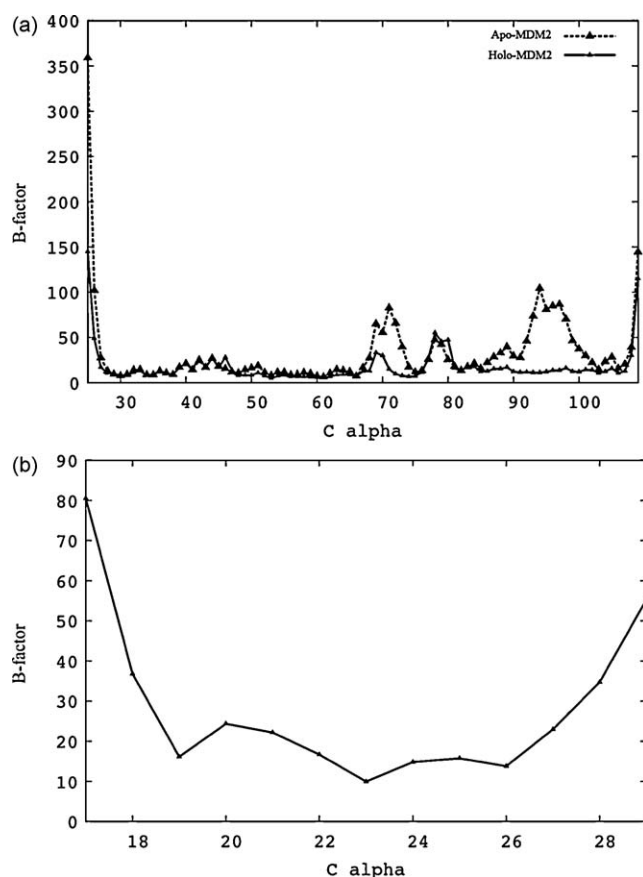


**Fig. 3.** Plot of the B-factors averaged over the protein backbone atoms as a function of residue number in the simulations of (a) MDM2-free and MDM2-bound and (b) p53 peptide. The solid and dotted lines correspond to MDM2-bound and MDM2-free, respectively.

localized protein movement, resulting in improved fit of the ligand. However, an obvious drawback when considering only the flexibility of restricted protein fragments is that the collective motion of the complete receptor backbone is neglected. To overcome this deficiency we have used an ensemble of protein conformations for docking as an alternative approach to introduce a feature of global protein flexibility. This ensemble could describe the entire conformational space of the binding site, yet must still be represented by a set of limited conformations in order to save computational screening time.

To generate a reduced set of representative models of the MDM2 binding site, we applied the RMSD conformational clustering to the apo-MDM2 and holo-MDM2 binding-site trajectories. Fig. 4 shows the evaluation of the Davies–Bouldin Index (DBI) and the percentage of variance explained by the data (SSR/SST) for different cluster counts (see Section 3). DBI for the apo-system exhibited local minima at cluster counts of 10, 20 and 60. However, as the percentage of variance explained by the data started to plateau after 45 clusters for the apo-system, we concluded that 60 clusters is a reasonable cut-off for the free-MDM2 structures. On the other hand, the correlation between these two criteria nicely occurred at a cluster count of 30 for the holo-structure.

In this study, we constructed an ensemble of 28 distinct conformations to perform ensemble-based virtual screening on MDM2 against the full set of ligand compounds. This ensemble incorporated the most dominant 22 structures that comprised ~75% of apo-trajectory, the most dominant five holo-structures that represented ~80% of the bound conformations (data not

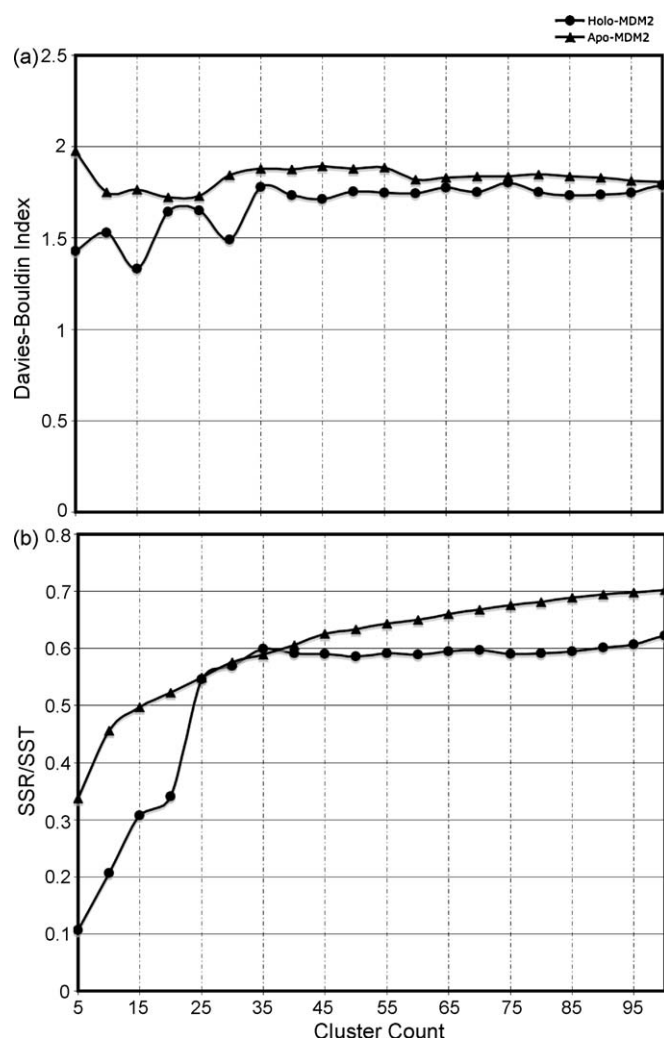


**Fig. 4.** Clustering analysis for the two MDM2 trajectories. A high-quality clustering is obtained when a local minimum in DBI correlates with saturation in the SSR/SST ratio. This is clear at cluster count of 60 for the apo-structure and 30 clusters for the holo-structure.

shown) and finally the MDM2 conformation extracted from the p53-bound crystal structure. The ultimate goal was to reduce the number of representative structures included in the ensemble-based screening and concurrently comprise most of the conformational space of the binding site. Fig. 5 represents the 28 structures used in this work. The MDM2 protein adopted diverse conformational changes demonstrating the significance of introducing receptor flexibility during the docking procedure.

#### 2.4. Pose clustering

As mentioned above, 28 independent virtual screening experiments were performed against the full set of database compounds. Screening of the full set of compounds contained in the NCIDS, DrugBank and the inhibitor-derivatives databases (more than 6000 molecules), against the 28 target structures, produced a total of ~19 million distinct poses that required classification. While AUTODOCK is capable of clustering these poses into subgroups depending on RMSD, the total number of clusters and the population of each cluster is mostly dependent on the RMSD cut-off that is initially chosen. As such, there is no adequate means to anticipate an optimum cut-off for the RMSD to produce the best quality result. Since we are dealing with a diverse set of input ligands, this clustering method does not provide an accurate means

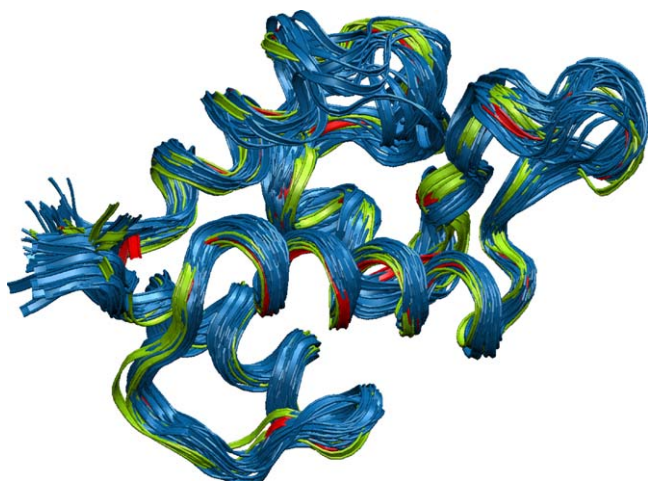


**Fig. 5.** Twenty-eight dominant conformations for MDM2. This ensemble comprised the crystal structure (red), five structures extracted from the holo-trajectory (green) and 22 structures extracted from the apo-trajectory (blue). (For interpretation of the references to color in this figure legend, the reader is referred to the web version of the article.)

of comparing resulting populations and binding energies between ligands, making it difficult to score compounds accurately.

The optimal number of clusters required for grouping similar conformations of a ligand in a typical docking run would depend on factors such as the binding mode, shape, and flexibility of the ligand. To be truly successful, a dynamic clustering technique must take full advantage of observable differences between the diverse conformations adopted by the ligand within the binding site. Moreover, it should adapt the cluster count to extract and make sense of the information inherited with these conformations. In this study, we automated the clustering approach used for clustering the MD trajectory (see Section 3) to extract the optimal number of clusters from docking results. This required a parameter to measure the quality of the clusters produced and to represent a convergence criterion for the clustering program. Of the various clustering metrics described in the literature, we used the elbow criterion as a measure for clustering convergence (see Section 3) due to its simple implementation. Also, visualization of the clustering is rapid and obvious. Here, we have applied this methodology by calculating the percentage of variance found within the data after each attempt to extract a new cluster from the system. As the number of clusters exceeds the optimal number, the percentage of variance should plateau indicating a complete extraction of the significant information included in the system.

#### 2.5. Ranking of MDM2-ensemble-based screening using AUTODOCK scoring function

For each virtual screening experiment, we have ranked significant poses for each of the 6617 molecules contained in the database by using the results from the elbow criterion and the lowest energy that corresponds to the most populated cluster. Once all poses from each ligand entry were clustered, we then filtered all of the clusters so that only those containing at least 25% of the total population were considered as top hits. Top hits were collected from the 28 experiments by first extracting the largest cluster from each individual screening followed by ranking the clusters according to their binding energies. This produced a set of non-redundant hits ranked by their binding energies of the most populated cluster. Top 300 hits were rescored using the MM–PBSA method (see below) and were used in the subsequent MDMX-screening.

#### 2.6. Ranking of MDM2 top hits using the MM–PBSA scoring function

It has been generally recognized that MD simulations can be useful as a post-docking tool in order to refine the final docked complexes and eliminate their impractical interactions. Although this procedure requires extensive computational resources, it tends to improve the protein–ligand interactions and enhance the complementarity between them. Moreover, the stability of the complexes over the simulation time is a direct measure of the consistency of binding, since improperly docked structures are expected to produce unstable trajectories. Finally, MD simulations provide a direct means to observe the role of water in mediating the contacts between the target and ligand molecules which help appreciate its effect on their binding.

While this procedure leads to the prediction of the correct conformation of the protein/ligand complexes by tolerating their induced fit interactions, another essential constraint for a successful VS experiment is to accurately predict their binding energies. This requires a consistent scoring method that can efficiently separate active from non-active compounds and classify the hits according to their relative binding. Here, we used the MM–PBSA method, introduced by Kollman et al. [43] to rescore the top 300 hits from the MDM2 screening and compare the predicted binding energies to the values obtained by the AUTODOCK scoring function. This technique has been previously adopted as an alternative approach to rescore docking results and shown to produce accurate free energies at a reasonable computational cost [56]. Its main advantages are the lack of adjustable parameters and the option of using a single MD simulation for the complete system to determine all energy values.

As has been reported by other groups, the most computationally demanding step is the calculation of the solute entropy using NMODE method. Although this component can be neglected if only relative binding (relative ranking) of compounds is required [43], we calculated the entropy contributions for all the top 300 hits using 200 snapshots extracted from their 2 ns MD trajectories (see Section 3). In our calculations, this part ranged from 20 to 30 kcal/mol, indicating its significance in predicating the overall binding energies.

The apparent  $IC_{50}$  values for Nutlin3, MI-219, TDP665759 and PMI in binding to MDM2 are 90 nM [18], 5 nM [18], 704 nM [18,29] and 3.4 nM [35] at 25°C, respectively. We did not find explicit values for the binding affinities of the three non-peptide molecules regarding their binding to MDMX, however, it has been experimentally confirmed that these compounds are weak binders to MDMX [18,29,35]. The  $IC_{50}$  values can be converted to the observed free energy change of binding,  $\Delta G$ , using the relation:

$$\Delta G = RT \ln K_i$$

where  $R$  is the gas constant,  $R = 1.987 \text{ cal K}^{-1} \text{ mol}^{-1}$  and  $T$  is the absolute temperature. Table 2 lists the estimated binding energies for the three compounds compared to the experimentally expected values. Due to the vast number of torsional degrees of freedom in the peptide structure, we did not use the AUTODOCK scoring function to calculate its binding energies to the two proteins. Although the discrepancy in the MM–PBSA calculations for the interactions of the four inhibitors with MDM2 is about 1 kcal/mol, the predicted values are in excellent agreement with the experimental data compared to the values obtained by the AUTODOCK scoring function. This observation is evident in the calculated values for their interactions with the MDMX target, predicting their weak binding to the protein. These results also illustrate the limitations of the AUTODOCK scoring function in eliminating false positive ligands, i.e. compounds that cannot practically bind but are predicted to bind, from active compounds. This is shown in Table 2, where the TDP665759 compound is predicted to bind to MDMX with a relatively high

**Table 2**

Relative ranking of positive controls using the two scoring methods compared to experimental data.

Compound	MDM2 ranking (kcal/mol)			MDMX ranking (kcal/mol)		
	MM/PBSA	AUTODOCK	Experimental	MM/PBSA	AUTODOCK	Experimental
MI-219	−10.6 ± 1.5	−9.1 ± 2.2	−11.4 [18]	−5.3 ± 1.5	−6.8 ± 2.2	−5.9 [18]
Nutlin3	−9.3 ± 1.3	−8.2 ± 2.2	−9.7 [18,35]	−6.1 ± 1.6	−5.8 ± 2.2	Negligible [35]
TDP665759	−9.5 ± 1.5	−9.1 ± 2.2	−8.4 [18,29]	−5.6 ± 1.4	−8.2 ± 2.2	Negligible [29]
PMI	−10.4 ± 1.6	N/A	−11.6 [35]	−12.8 ± 1.5	N/A	−11.5 [35]

**Table 3**

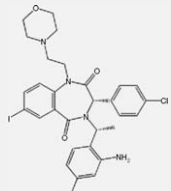
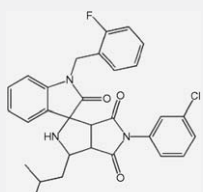
MDM2 top hits. The top 20 hits from MDM2 screening ranked by their binding energies as were calculated using the MM–PBSA method and compared to their ranking using the AUTODOCK scoring function.

MM–PBSA scoring		Ensemble-based scoring		ID
Rank	BE (kcal/mol)	Rank	BE (kcal/mol)	
1	−14.1	97	−9.2	ZINC08552001
2	−14.1	101	−9.2	NSC#82892
3	−14.0	42	−9.7	Pub#11952783
4	−13.8	187	−9.0	Pub#11375913
5	−13.2	285	−8.5	Pub#10312264
6	−13.0	175	−8.9	Pub#25055003
7	−12.8	191	−8.8	NSC#59276
8	−12.6	293	−8.5	Pub#456323
9	−11.7	110	−9.1	Pub#11855975
10	−11.4	80	−9.3	Pub#11952782
11	−11.3	115	−9.1	Pub#22721132
12	−11.3	150	−9.0	NSC#409664
13	−11.3	81	−9.3	Pub#21060012
14	−11.0	232	−8.7	Pub#20726116
15	−10.9	127	−9.0	Pub#22632481
16	−10.9	267	−8.6	Pub#11272250
17	−10.8	62	−9.5	Pub#22720968
18	−10.8	180	−8.8	NSC#77037
19	−10.6	109	−9.1	MI-219
20	−10.6	93	−9.2	Pub#22721012

binding energy compared to the rest of the compounds. On the other hand, the MM–PBSA approach selected the real binders for the two protein targets. For MDM2, the four ligands can bind strongly to the protein, while, for MDMX, only the PMI peptide can bind with a very high binding energy. This also explains the variations between the two scoring methods in ranking the compounds (see Tables 3–5).

**Table 5**

MDMX/MDM2-inhibitors. The listed compounds are predicted to bind to the MDM2 and MDMX proteins. The compounds are ranked by their binding energies as were calculated using the MM–PBSA method.

MDMX rank		MDM2 rank		ID	Structure
Rank	BE (kcal/mol)	Rank	BE (kcal/mol)		
5	−12.5	11	−11.3	Pub#11952782	
10	−10.9	45	−8.8	Pub#5039349	

**Table 4**

MDMX-specific top hits. Compounds are ranked by their binding energies as were calculated using the MM–PBSA method and compared to their ranking using the AUTODOCK scoring function. The listed compounds have been predicted to bind to MDMX and not to MDM2.

MM–PBSA scoring		Ensemble-based scoring		ID
Rank	BE (kcal/mol)	Rank	BE (kcal/mol)	
1	−13.2	277	−5.5	ZINC12503171
2	−13.1	74	−7.8	NSC#72254
3	−12.9	178	−7.1	Pub#20726118
4	−12.8	N/A	N/A	PMI
6	−11.6	111	−7.5	Pub#11455269
7	−11.5	13	−8.5	Pub#22721034
8	−11.3	69	−7.8	Pub#10196974
9	−11.0	100	−7.6	Pub#22720998
11	−10.7	43	−8.1	Pub#10290053
13	−10.4	130	−7.4	Pub#22721115
16	−9.9	30	−8.2	Pub#22721175
17	−9.9	50	−8.1	Pub#11541499
18	−9.8	226	−6.7	Pub#11614489
19	−9.7	41	−8.2	Pub#22721095
21	−9.5	19	−8.4	Pub#22721184
22	−9.53	25	−8.3	Pub#216345
23	−9.41	191	−7.0	Pub#24788704
24	−9.35	121	−7.5	Pub#20726117
25	−9.29	57	−7.9	ZINC08552003
29	−9.19	184	−7.1	Pub#17754804

As the MM/PBSA confirmed the experimental findings, our subsequent step was to use this technique to rescore the top hits obtained by the AUTODOCK scoring function. Table 3 shows the top 20 hits obtained from the ensemble-based screening after rescoring their interactions using the MM–PBSA method. Although Nutlin3 and TDP665759 are not shown in this table, the ranks of the two compounds were 41 and 36, respectively. It should also be

Table 5 (Continued)

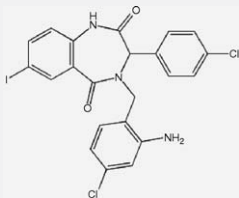
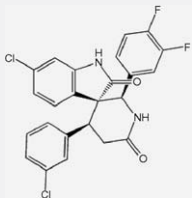
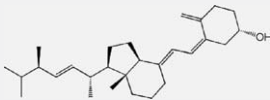
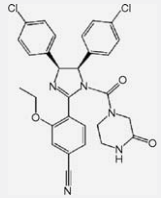
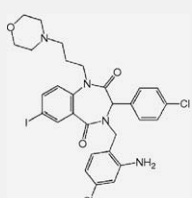
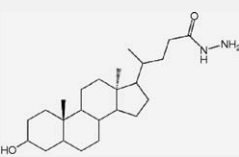
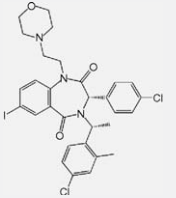
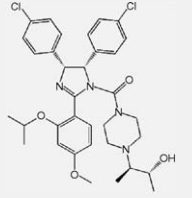
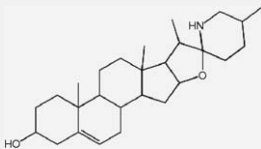
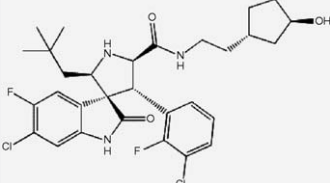
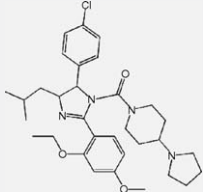
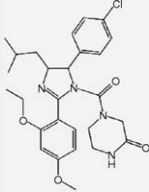
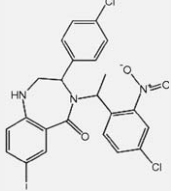
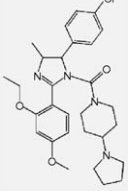
MDMX rank		MDM2 rank		ID	Structure
Rank	BE (kcal/mol)	Rank	BE (kcal/mol)		
12	−10.5	67	−7.5	Pub#11284279	
14	−10.2	69	−7.4	Pub#24788253	
15	−10.0	62	−7.7	ZINC04629876	
20	−9.6	10	−11.7	Pub#11855975	
26	−9.3	50	−8.3	Pub#11953191	
28	−9.2	45	−8.7	NSC#73109	
31	−9.0	39	−9.0	Pub#11952569	
32	−8.7	65	−7.5	Pub#10240227	



Table 5 (Continued)

MDMX rank		MDM2 rank		ID	Structure
Rank	BE (kcal/mol)	Rank	BE (kcal/mol)		
38	−8.2	49	−8.4	NSC#179187	
43	−8.0	7	−13.0	Pub#25055003	
45	−8.0	44	−7.2	Pub#11753378	
47	−7.7	17	−10.9	Pub#11272250	
49	−7.6	25	−10.3	Pub#21934780	
60	−7.0	4	−13.8	Pub#11375913	

mentioned that a considerable number of the compounds showed positive binding energies after rescoring them using the MM/PBSA method (data not shown), supporting the ability of this technique to discriminate inactive compounds from the AUTODOCK suggested hits. Although most of the top 20 hits are derivatives of the three positive controls, in particular the benzodiazepinedione scaffold (TDP665759), 5 compounds from both the NCI diversity set and DrugBank libraries showed strong binding energies compared to the positive controls.

### 2.7. Screening of MDM2 top hits against MDMX

The top 300 hits which resulted from the ensemble-based screening were then docked to an equilibrated MDMX structure that was extracted from the PMI/MDMX complex (see Section 3). The

docking step was essential in order to place the compounds within the p53-binding site with their minimum energy conformation. Following the procedure described above, we used the MM/PBSA method to predict the absolute binding energies for each compound. Reassuringly, our calculations confirmed the experimental findings, where the three non-peptidic positive controls showed weak binding to MDMX compared to MDM2 while the PMI peptide showed very high binding energy (see Table 2). Analogously to the experimental results concerning the high specificity of these molecules to the MDM2 target, our calculations predict that a number of compounds can also bind more strongly to MDMX than to MDM2. The top 20 hits selected from these compounds are expected to be specific MDMX-inhibitors and are shown in Table 4.

Table 5 lists the compounds that are suggested to function as dual-MDM2/MDMX-inhibitors obtained from screening the top

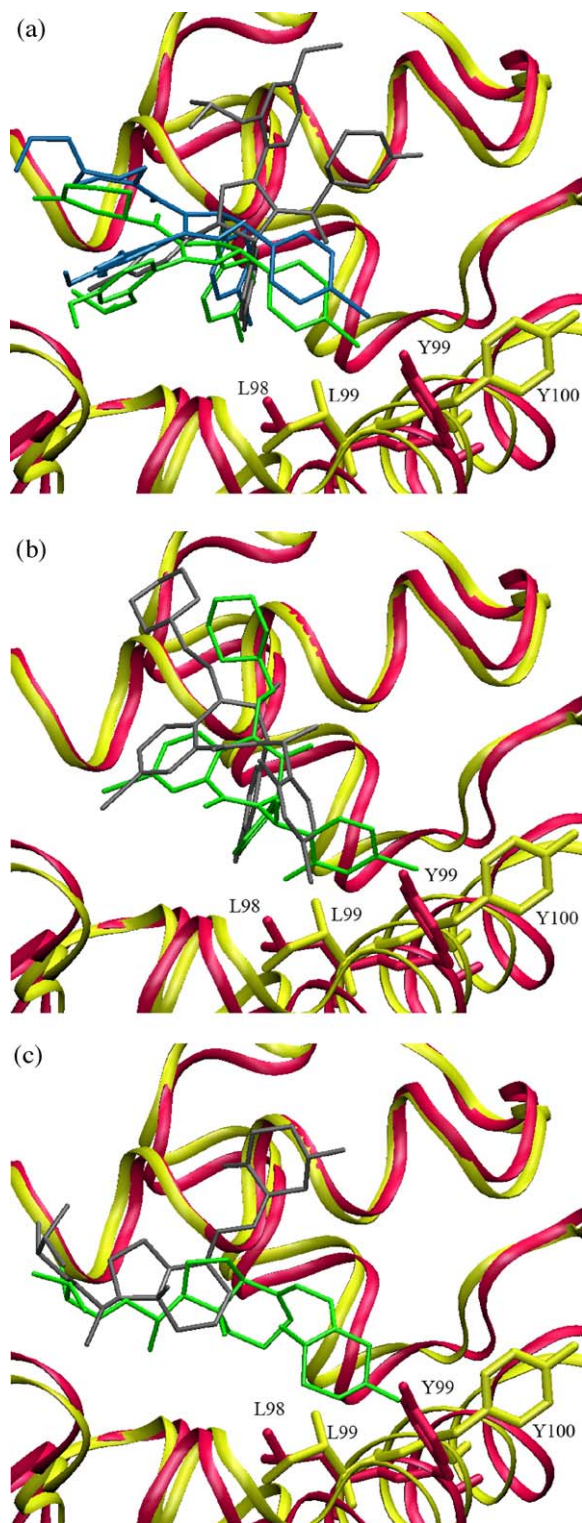


**Fig. 6.** Structural variations between MDM2 (yellow) and MDMX (red) and their effect on the binding modes of Nutlin3 (a) and two selected hits from the predicted MDM2/MDMX-inhibitors (b and c). Tyr100 and Leu99 of MDM2 and the same residues in MDMX are shown in Licorice representations with the same color as that of the two proteins. For each compound, the binding mode within MDM2 is shown in green and within MDMX is shown in gray. Tyr99 and Leu98 prevent Nutlin3 from binding to MDMX with the same binding conformation adopted by Nutlin2 within the MDM2-pocket (blue). The conformation of Nutlin2 was extracted from the MDM2–Nutlin crystal structure 1RV1. On the other hand, compounds Pub#11952782 (b) and ZINC04629876 (c) from the suggested MDM2/MDMX-inhibitor list can tolerate the structural variations in the two binding sites in order to maximize their interactions with the proteins. (For interpretation of the references to color in this figure legend, the reader is referred to the web version of the article.)

MDM2-hits against the p53-binding site within the MDMX target. Here, we used MM-PBSA energies to compare the binding of these hits to the two target proteins. As we are only interested in compounds that can bind to MDM2 with affinities as good as those of the known MDM2-inhibitors, we limited our selection to the 16 compounds shown below (see Table 5). Although the binding sites are fairly similar, the MDMX pocket seems to be more compact than that of MDM2. This is mainly due to the three residues Pro95, Ser96 and Pro97 in MDMX that have been replaced by His96, Arg97 and Lys98 in MDM2. These substitutions are located on one of the alpha helices that comprise the p53-binding site within the two proteins. Consequently, the proline residues (Pro95 and Pro97) in MDMX shift this helical domain in MDMX relative to MDM2 and cause Lys98 and Tyr99 to protrude into the p53-binding cleft within MDMX, making it shallower and less accessible to many of the MDM2 top hits we found. Moreover, we noticed very minor differences in the electrostatic potential distributions around the surfaces of the two proteins (data not shown), where MDM2 is more positively charged in certain regions deeply located within the binding site. These slight variations in both shape and electrical properties of the two proteins played a considerable role in governing the final conformation adopted by the ligands. This observation is clear when comparing the binding modes of Nutlin within the two pockets (see Fig. 6a). While Tyr100 and Leu99 of MDM2 extend the binding site allowing Nutlin to intimately bind to MDM2, the same residues in MDMX clash with the drug preventing it from taking the normal conformation that was adopted within MDM2. On the other hand, Fig. 6b and c show how two compounds from the list of proposed MDM2/MDMX-inhibitors were able to tolerate the structural variations between the two binding sites. This is apparent in Fig. 6, where the compounds took on different conformations within the two binding pockets in order to maximize their interactions with the proteins.

### 3. Methods and materials

#### 3.1. Molecular dynamics simulations

The amino-terminal domain of MDM2 (residues 25–109) bound to a 13-residue transactivation domain peptide of p53 (residues 17–29) was taken from PDB entry 1YCR [8]. MD simulations were carried out using the NAMD program [44] at a mean temperature of 310 K and physiological pH (pH 7) using the all-hydrogen AMBER99SB force field [45]. Protonation states of all ionizable residues were calculated using the program PDB2PQR [46]. Following parameterization, the MDM2 protein alone (subsequent to removing the p53 peptide from the p53–MDM2 crystal structure) or in complex with the p53 peptide was immersed in the center of TIP3P water cube after adding hydrogen atoms to the initial protein structure. The cube dimensions were chosen to provide at least a 20 Å buffer of 12,724 (12,653) water molecules around the systems. To neutralize and prepare the p53-bound or (free) systems under a physiological ionic concentration, 30 (28) chloride and 23 (23) sodium ions were respectively added by replacing water molecules having the highest electrostatic energies on their oxygen atoms. The number of counter ions for each case was calculated by first estimating the amount of ions that is needed to set up the system under normal physiological conditions (pH 7), followed by adding the number of chloride ions required to bring its charge to zero. The fully solvated protein was then minimized and subsequently heated to the simulation temperature with heavy restraints placed on all backbone atoms. Following heating, the system was equilibrated using periodic boundary conditions for 100 ps and energy restraints reduced to

zero in successive steps of the MD simulation. The simulations were then continued for 55 (78) ns during which atomic coordinates were saved to the trajectory every 2 ps. The total simulation time was determined by visualizing the quality of sampling as predicted by PCA (see below). The RMSD and B-factors for the protein backbone were then computed over the last 10 ns of the MD simulation using the PTRAJ utility within AMBER10 [47]. Hydrogen bond analyses were performed by computing the average distance between donor and acceptor atoms. A hydrogen bond was defined by a heavy donor–heavy acceptor distance  $\leq 3.4$  Å, a light donor–heavy acceptor distance  $\leq 2.5$  Å, and a deviation of less than  $\pm 60^\circ$  from linearity.

Following the same MD protocol mentioned above we prepared two equilibrated models for the PMI/MDM2 (PDB entry: 3EQS) [35] and PMI/MDMX (PDB entry 3EQY) [35] complexes. Parameters for ligands were assigned using the generalized AMBER force field [48] and partial charges were calculated with the AM1-BCC method [49] using Antechamber in the AMBER 10 package. Following parameterization, the protein/ligand complexes were subjected to the same MD protocol we used before (see above) for a production phase of 2 ns. Snapshots were extracted every 2 ps and used for the MM/PBSA binding energy analysis.

### 3.2. RMSD clustering to extract representative MD structures

MD simulations on the free and bound MDM2 systems produced numerous structures that explored their conformational space. Although performing VS against each snapshot of these trajectories is the most accurate way to account for full receptor flexibility, implementing this technique is unfeasible and requires massive computational resources. A suitable way to accommodate receptor flexibility and concurrently, reduce the required computations is to dock the ligand library against a set of representative structures that describes the conformational space of the target [50,51,39]. Although this approach significantly reduces the number of VS experiments, care should be taken in extracting these representative structures. A common approach to generate such ensemble of representative models is to perform RMSD conformational clustering on the whole trajectory [50]. Unfortunately, there is no universally accepted clustering algorithm that can be used to extract all of the information contained within the MD simulation. However, recent studies suggest that a number of clustering algorithms, such as average-linkage, means and self-organizing maps (SOM) can be used in clustering MD data [52]. The clustering quality can be anticipated by calculating a number of clustering metrics that can deduce the optimal number of clusters to be extracted and their population size. These are the Davies–Bouldin index (DBI) [53] and the “elbow criterion” [52]. A high-quality clustering scheme is expected when high DBI values are calculated. On the other hand, using the elbow criterion, the percentage of variance explained by the data, is expected to plateau for cluster counts exceeding the optimal number [52]. Using these metrics, by varying the number of clusters, one should expect for adequate clustering, a local minimum for DBI and a horizontal line for the percentage of variance explained by the data.

To generate a reduced set of representative MDM2 models, we performed RMSD conformational clustering with the average-linkage algorithm as implemented in the PTRAJ utility of AMBER10 using cluster counts ranging from 5 to 100 clusters. For the two MDM2 simulations, structures were extracted at 2 ps intervals over the entire simulation times. All  $C_\alpha$ -atoms were RMSD fitted to the minimized initial structure in order to remove overall rotation and translation. RMSD clustering was performed on the 18 residues that line the p53-binding cleft within MDM2, namely those numbered: 25, 26, 50, 51, 54, 58, 61, 62, 67, 72, 73,

93, 94, 96, 97, 99, 100, 104. These residues were clustered into groups of similar conformations using the atom-positional RMSD of the entire amino acid, including side chains and hydrogen atoms, as the similarity criterion. The optimal numbers of clusters for the two systems were chosen after evaluation of the two clustering metrics, described above, for different cluster counts (see Section 2). Sixty clusters were obtained for the apo-MDM2, while 30 clusters were extracted for the holo-MDM2. The centroid of each cluster, the structure having the smallest RMSD to all members of the cluster, was chosen as the cluster representative structure and the most dominant structures were used as rigid templates for the ensemble-based docking experiments (see Section 2).

### 3.3. Principal Component Analysis

PCA can transform the original space of correlated variables from a large MD simulation into a reduced space of independent variables comprising the essential dynamics of the system [54,55]. For a typical protein, the system's dimensionality is thereby reduced from tens of thousands to fewer than fifty degrees of freedom. To perform PCA for a subset of  $N$  atoms, the entire MD trajectory is RMSD fitted to a reference structure, in order to remove all rotations and translations. The covariance matrix can then be calculated from their Cartesian atomic coordinates as:

$$\sigma_{ij} = \langle (r_i - \langle r_i \rangle)(r_j - \langle r_j \rangle) \rangle \quad (1)$$

where  $r_i$  represents one of the three Cartesian co-ordinates ( $x_i$ ,  $y_i$  or  $z_i$ ) and the eigenvectors of the covariance matrix constitute the essential vectors of the motion. It is generally accepted that the larger an eigenvalue, the more important its corresponding eigenvector in the collective motion. PCA can also be employed to predict the completeness of sampling during the MD simulation. A method proposed by Hess [57] divides an MD trajectory into separate parts, and their normalized overlap is calculated using the covariant matrices for each pair of parts:

$$\text{Normalized overlap } (C_1, C_2) = 1 - \frac{\sqrt{\text{tr}((\sqrt{C_1} - \sqrt{C_2})^2)}}{\sqrt{\text{tr}(C_1) + \text{tr}(C_2)}} \quad (2)$$

where  $C_1$  and  $C_2$  are the covariant matrices, and the symbol  $\text{tr}$  is used to denote the trace operation. If the overlap is 0, then the two sets are considered to be orthogonal, whereas an overlap of 1 indicates that the matrices are identical. To ensure completeness of sampling for MD simulations of MDM2, PCA of the binding-site residues was performed using the positions of all heavy atoms. The MD trajectory was divided into three parts and the normalized overlap between each pair was calculated to determine the completeness of sampling.

### 3.4. Selection of ligand database

The National Cancer Institute Diversity Set (NCIDS) [58], DrugBank small molecules [59] and a set of 3168 derivative structures for Nutlin3, MI-219 and TDP665759 were used as our test libraries of compounds. The NCIDS is a collection of approximately 2000 compounds that are structurally representative of a wide range of molecules, representing almost 140,000 compounds that are available for testing at the NCI. Unfortunately, a number of ligands containing rare earth elements could not be properly parameterized and were excluded, leaving a total of 1,883 compounds for analysis. Here, we used a version of the NCIDS formatted for use in AUTODOCK and was prepared by the AUTODOCK Scripps team. The DrugBank small molecule library



is a set of 1488 FDA-approved small-molecule drugs downloaded from the ZINC database. Some of these molecules were present in more than one protonation state adding another 78 structures to the docked ligands. We also appended the set of derivative structures of MDM2-inhibitors to the docked compounds for two reasons. First, we wanted to build upon the intensive efforts that have been previously made and incorporate variations in the original structures for these inhibitors in order to improve their performance in binding to MDM2 and MDMX. Moreover, since we search for dual-MDM2/MDMX-inhibitors, we expect that due to the structural similarity of the p53-binding sites within the two proteins, an MDMX-inhibitor should be a derivative structure of the known MDM2-inhibitors. Based on this assumption, we created a library of 3168 derivative structures similar to Nutlin3, MI-219, and TDP665759 by searching the PubChem [60] database and then extracting the results using a similarity threshold of  $\geq 90\%$ . Compounds similar to the query structure are measured using the Tanimoto score [61]. A Tanimoto score of 100% represents an “exact match” to the provided chemical structure query, while a value of 0% results in the return of all chemical structures deposited in the PubChem database. The threshold of  $\geq 90\%$  is chosen for efficiency of search since similarity links in PubChem are pre-computed at this value. Also, at this threshold, the compounds that are returned by the search would not be very close to the original query structure and yet provide reasonable number of chemical structures for this work. Therefore, the full set of ligands used in this study comprised 6617 different compounds.

#### 3.4.1. Ligand screening

Virtual screening on the p53-binding sites within MDM2 and MDMX was performed using AUTODOCK, version 4.0 [42]. Hydrogen atoms were added to MDM2, MDMX and ligands and partial atomic charges were then assigned using the Gasteiger–Marsili [62] method. Atomic solvation parameters were assigned to the atoms of the protein using the AUTODOCK 4.0 utility ADDSOL. Docking grid maps with  $126 \times 108 \times 126$  points and grid point spacing of 0.21 Å were then centered on the p53-binding site within the MDM2 and MDMX receptors using AUTOGUID4.0 program [42]. Rotatable bonds of each ligand were then automatically assigned using AUTOTORS utility of AUTODOCK4.0. Docking was performed using the Lamarckian Genetic Algorithm (LGA) method with an initial population of 400 random individuals; a maximum number of  $10 \times 10^6$  energy evaluations; 100 trials; 50,000 maximum generations; a mutation rate of 0.02; a crossover rate of 0.80 and the requirement that only one individual can survive into the next generation. A total of 28 independent virtual screening runs were performed against the full set of docked ligands with all residues of the receptors set kept rigid during docking experiments. This set of MDM2 models comprises one structure that represents the minimized holo-crystal conformation of MDM2, 22 conformations that represent  $\sim 80\%$  of the apo-MDM2 trajectory and five models that constitute  $\sim 75\%$  of the holo-MDM2 trajectory (see Section 2). We also performed a VS run on an equilibrated model for MDMX using the top 300 MDM2-hits resulted from the ensemble-base screening.

#### 3.4.2. Clustering of docked poses

The previously described virtual screening experiments involved millions of conformations of each ligand bound to MDM2. AUTODOCK can cluster these output poses into subgroups depending on their RMSD values referred to a reference structure. Although this approach shows the possible binding modes of a ligand to the binding site, the number of clusters and the population size for each cluster depends heavily on the RMSD

cut-off used. It is not possible to anticipate an optimum cut-off for the RMSD in order to produce a clustering pattern with the highest confidence, motivating us to use alternative approaches in performing the clustering analysis. In this study, we used an automated approach to couple one of the commonly used clustering metrics, the elbow criterion [52], with the clustering module of PTRAJ utility of AMBER10. This method exploits the fact that the percentage of variance explained by the data ( $\lambda$ ), is expected to plateau for cluster counts exceeding the optimal number.

The percentage of variance is defined by:

$$\lambda = \frac{SSR}{SST} \quad (3)$$

where SSR is the sum-of-squares regression from each cluster summed over all clusters and SST is the total sum-of-squares. Here, we used the SOM algorithm, as implemented in the PTRAJ utility of the AMBER10 program, to cluster the docking results. This modified clustering program increases the number of clusters required until the percentage of variance explained by the data ( $\lambda$ ) plateaus. This can be determined by calculating the first and second derivatives of the percentage of variance with respect to the clusters number ( $d\lambda/dN$  and  $d^2\lambda/dN^2$ ) after each attempt to increase the cluster counts. The clustering process then stops at an acceptable value for these derivatives that is close to 0. Consequently, the clustering procedure depends only on the system itself and adjusts itself to arrive at the optimal clustering pattern for that specific system.

#### 3.5. Rescoring of top hits using MM–PBSA

Binding free energies were calculated using the molecular mechanics Poisson–Boltzmann surface area (MM–PBSA) method [43] as implemented in AMBER10. The total free energy is the sum of average molecular mechanical gas-phase energies ( $E_{MM}$ ), solvation free energies ( $G_{solv}$ ), and entropy contributions ( $-TS_{solute}$ ) of the binding reaction:

$$G = E_{MM} + G_{solv} - TS_{solute} \quad (4)$$

In this work, the molecular mechanical ( $E_{MM}$ ) energy of each snapshot was calculated using the SANDER module of AMBER10 with all pair-wise interactions included using a dielectric constant ( $\epsilon$ ) of 1. The solvation free energy ( $G_{solv}$ ) was estimated as the sum of electrostatic solvation free energy, calculated by the finite-difference solution of the Poisson–Boltzmann equation in the Adaptive Poisson–Boltzmann Solver (APBS) program as implemented in AMBER10 and non-polar solvation free energy, calculated from the solvent-accessible surface area (SASA) algorithm. The solute entropy was approximated using the normal mode analysis. Applying the thermodynamic cycle for each ligand–MDM2/MDMX complex, the binding free energy between an arbitrary ligand molecule and the MDM2/MDMX protein can be approximated by:

$$\Delta G^\circ = \Delta G_{gas}^{MDM2/MDMX-ligand} + \Delta G_{solv}^{MDM2/MDMX-ligand} - \{ \Delta G_{solv}^{ligand} + \Delta G_{solv}^{MDM2/MDMX} \} \quad (5)$$

Here, ( $\Delta G_{gas}^{MDM2-ligand}$ ) represents the free energy per mole for the non-covalent association of the ligand–MDM2 complex in vacuum (gas phase) at 300 K, while ( $-\Delta G_{solv}$ ) stands for the work required to transfer a molecule from its solution conformation to the same conformation in vacuum at 300 K (assuming that the binding conformation of the ligand–MDM2 complex is the same in solution and in vacuum).



#### 4. Conclusions

The tumor suppressor p53 is one of the most frequently inactivated proteins in human cancers. Direct gene modifications in p53 gene, *Tp53*, or the interaction between p53 and its two major cellular inhibitors, MDM2 and MDMX, are two fundamental mechanisms employed by cancer cells to block the p53 pathway [1–4]. Over a number of years, leading efforts in p53 research have been focused on restoring the activity of the mutant protein as a precursor to developing a novel cancer treatment. Although these studies revealed the prospects of inducing tumor cell death, the development of a non-peptide small-molecule p53-activator is still a particularly challenging problem [69,70]. Other significant efforts in this area have been aimed at the discovery of small-molecule inhibitors that can disrupt the interaction of p53 with its main cellular regulator, MDM2 [18–21]. This led to the development of Nutlin3 [22] and MI-219 [23], the most potent and specific non-peptide MDM2-inhibitors discovered so far.

Recently, MDMX, a protein homologous to MDM2, was found to reduce the efficacy of MDM2-inhibitors including Nutlin3 [18,34]. This suggested MDMX as a new attractive therapeutic target and indicated a need to develop MDMX-specific or MDM2/MDMX dual-inhibitors to fully-activate the p53 pathway in tumor cells expressing wild-type p53.

Here, we used an improved relaxed complex Scheme 39 by combining MD simulations and molecular docking with binding energy analysis to filter a set of 6617 compounds for effective inhibitors of MDM2 and MDMX. These compounds included the NCI diversity set [58], DrugBank small molecules [59] and a newly generated set of ~3000 derivative structures similar to known MDM2-inhibitors. The derivative library of compounds was included among the docked structures because the structural similarity between the two proteins would imply that an MDMX-inhibitor should be a derivative structure based on one of the known MDM2-inhibitors. Although, more than 6000 compounds have been screened in this study, we suggest the use of larger libraries (in the order of 100,000 to 1,000,000 compounds) will be more effective in discovering more active hits in future work. In this context, we used MD simulations, principle component analysis and an iterative clustering technique to generate an ensemble of 28 MDM2 structures that characterize the collective dynamics of the MDM2 protein. Then, we used molecular docking to explore the conformational space of the ligands and to search for their minimal energy configuration within the MDM2 binding site. All docking poses were clustered using the same iterative procedure that we used in extracting the protein structures and then sorted with the minimal energy of the largest cluster. The top 300 hits were rescored using the MM-PBSA procedure and prepared for a second round of screening against the MDMX target. Following the docking of MDM2-hits to MDMX we used the MM-PBSA technique to rescore their binding affinities to MDMX and suggest a set of MDM2/MDMX dual-inhibitors.

Our results confirmed the experimental findings concerning the weak binding of the MDM2-inhibitors Nutlin3, MI-219 and TDP to its homolog structure MDMX. Moreover, as we anticipated, the top hits from our screening are primarily derivative structures of the three known inhibitors. However, we also suggested a few structures from the NCI diversity set and DrugBank compounds. The molecules we have proposed in the present study, can fit within the two binding sites and adopt different conformations to maximize their interactions with the two proteins. We have also validated our top hit list by comparing their estimated binding energies to the PMI peptide, an MDM2/MDMX dual-inhibitor proposed by Pazgier et al. [35] and, reassuringly, our top hits are predicted to have comparable performance to this peptide. It is hoped that our findings will facilitate the development of a new

generation of MDM2/MDMX dual-inhibitors that would fully-activate the p53 pathway and offer new hope in the fight against a broad range of cancers.

#### Acknowledgments

All of the molecular dynamics simulations and virtual screening experiments were produced using the SHARCNET, AICT (University of Alberta cluster) and WESTGRID computational facilities. Funding for this work was obtained from the Alberta Cancer Foundation, the Allard Foundation and NSERC. JAT wishes to thank Prof. A. Fersht of Cambridge University for bringing this problem to his attention.

#### References

- [1] J.G. Teodoro, S.K. Evans, M.R. Green, Inhibition of tumor angiogenesis by p53: a new role for the guardian of the genome, *J. Mol. Med.* 85 (2007) 1175.
- [2] J.S. Fridman, S.W. Lowe, Control of apoptosis by p53, *Oncogene* 22 (2003) 9030.
- [3] K.H. Vousden, X. Lu, Live or let die: the cell's response to p53, *Nat. Rev. Cancer* 2 (2002) 594.
- [4] J.C. Bourdon, V.D. Laurenzi, G. Melino, D. Lane, p53: 25 years of research and more questions to answer, *Cell Death Differ.* 10 (4) (2003) 397.
- [5] B. Vogelstein, D. Lane, A.J. Levine, Surfing the p53 network, *Nature* 408 (2000) 307.
- [6] A. Feki, I. Irminger-Finger, Mutational spectrum of p53 mutations in primary breast and ovarian tumors, *Crit. Rev. Oncol. Hematol.* 52 (2004) 103.
- [7] M.H. Kubbutat, S.N. Jones, K.H. Vousden, Regulation of p53 stability by Mdm2, *Nature* 387 (1997) 299.
- [8] P.H. Kussie, et al., Structure of the MDM2 oncoprotein bound to the p53 tumor suppressor transactivation domain, *Science* 274 (1996) 948.
- [9] S.S. Fakhrazadeh, S.P. Trusko, D.L. George, Tumorigenic potential associated with enhanced expression of a gene that is amplified in a mouse tumor cell line, *EMBO J.* 10 (1991) 1565.
- [10] J.D. Oliner, K.W. Kinzler, P.S. Meltzer, D.L. George, B. Vogelstein, Amplification of a gene encoding a p53-associated protein in human sarcomas, *Nature* 358 (1992) 80.
- [11] J. Momand, D. Jung, S. Wilczynski, J. Niland, The MDM2 gene amplification database, *Nucleic Acids Res.* 26 (1998) 3453.
- [12] A. Shvarts, W.T. Steegenga, N. Riteco, T. van Laar, P. Dekker, M. Bazuine, R.C. van Ham, W. van der Houven van Oordt, G. Hateboer, A.J. van der Eb, A.G. Jochemsen, MDMX: a novel p53-binding protein with some functional properties of MDM2, *EMBO J.* 15 (1996) 5349.
- [13] M.W. Jackson, S.J. Berberich, MdmX protects p53 from Mdm2-mediated degradation, *Mol. Cell. Biol.* 20 (2000) 1001.
- [14] F. Toledo, K.A. Krummel, C.J. Lee, C.W. Liu, L.W. Rodewald, M. Tang, G.M. Wahl, A mouse p53 mutant lacking the proline-rich domain rescues Mdm4 deficiency and provides insight into the Mdm2-Mdm4-p53 regulatory network, *Cancer Cell* 9 (2006) 273.
- [15] D.A. Sharp, S.A. Kratowicz, M.J. Sank, D.L. George, Stabilization of the MDM2 oncoprotein by interaction with the structurally related MDMX protein, *J. Biol. Chem.* 274 (1999) 38189.
- [16] Y. Pan, J. Chen, MDM2 promotes ubiquitination and degradation of MDMX, *Mol. Cell. Biol.* 23 (2003) 5113.
- [17] V. Böttger, C. Garcia-Echeverria, Y.F. Ramos, A.J. van der Eb, A.G. Jochemsen, D.P. Lane, Comparative study of the p53-mdm2 and p53-MDMX interfaces, *Oncogene* 18 (1999) 189.
- [18] S. Shangary, S. Wang, Targeting the MDM2-p53 interaction for cancer therapy, *Clin. Cancer Res.* 14 (2008) 5318.
- [19] L.T. Vassilev, MDM2 inhibitors for cancer therapy, *Trends Mol. Med.* 13 (2007) 23.
- [20] J.K. Buolamwini, J. Addo, S. Kamath, S. Patil, D. Mason, M. Ores, Small molecule antagonists of the MDM2 oncoprotein as anticancer agents, *Curr. Cancer Drug Targets* 5 (1) (2005) 57.
- [21] S. Patel, M.R. Player, Small-molecule inhibitors of the p53-MDM2 interaction for the treatment of cancer, *Expert Opin. Investig. Drugs* 17 (12) (2008) 1865.
- [22] L.T. Vassilev, Small-molecule antagonists of p53-MDM2 binding: research tools and potential therapeutics, *Cell Cycle* 3 (2004) 419.
- [23] K. Ding, Y. Lu, Z. Nikolovska-Coleska, S. Qiu, Y. Ding, W. Gao, J. Stuckey, K. Krajewski, P.P. Roller, Y. Tomita, D.A. Parrish, J.R. Deschamps, S. Wang, Structure-based design of potent nonpeptide MDM2 inhibitors, *J. Am. Chem. Soc.* 127 (2005) 10130.
- [24] S.G. Dastidar, D.P. Lane, C.S. Verma, Multiple peptide conformations give rise to similar binding affinities: molecular simulations of p53-MDM2, *J. Am. Chem. Soc.* 130 (41) (2008) 13514.
- [25] S. Shangary, D. Qin, D. McEachern, M. Liu, R.S. Miller, S. Qiu, Z. Nikolovska-Coleska, K. Ding, G. Wang, J. Chen, D. Bernard, J. Zhang, Y. Lu, Q. Gu, R.B. Shah, K.J. Pienta, X. Ling, S. Kang, M. Guo, Y. Sun, D. Yang, S. Wang, Temporal activation of p53 by a specific MDM2 inhibitor is selectively toxic to tumors and leads to complete tumor growth inhibition, *Proc. Natl. Acad. Sci. U.S.A.* 105 (2008) 3933.
- [26] K. Ding, Y. Lu, Z. Nikolovska-Coleska, G. Wang, S. Qiu, S. Shangary, W. Gao, D. Qin, J. Stuckey, K. Krajewski, P.P. Roller, S. Wang, Structure-based design of spirooxindoles as potent, specific small-molecule inhibitors of the MDM2-p53 interaction, *J. Med. Chem.* 49 (2006) 3432.

- [27] B.L. Grasberger, T. Lu, C. Schubert, D.J. Parks, T.E. Carver, H.K. Koblish, M.D. Cummings, L.V. LaFrance, K.L. Milkiewicz, R.R. Calvo, D. Maguire, J. Lattanze, C.F. Franks, S. Zhao, K. Ramachandren, G.R. Bylebyl, M. Zhang, C.L. Manthey, E.C. Petrella, M.W. Pantoliano, I.C. Deckman, J.C. Spurlino, A.C. Maroney, B.E. Tomczuk, C.J. Molloy, R.F. Bone, Discovery and cocrystal structure of benzodiazepinedione HDM2 antagonists that activate p53 in cells, *J. Med. Chem.* 48 (2005) 909.
- [28] D.J. Parks, L.V. LaFrance, R.R. Calvo, K.L. Milkiewicz, V. Gupta, J. Lattanze, K. Ramachandren, T.E. Carver, E.C. Petrella, M.D. Cummings, D. Maguire, B.L. Grasberger, T. Lu, 1,4-Benzodiazepine-2,5-diones as small molecule antagonists of the HDM2-p53 interaction: discovery and SAR, *Bioorg. Med. Chem. Lett.* 15 (2005) 765–770.
- [29] H.K. Koblish, S. Zhao, C.F. Franks, R.R. Donatelli, R.M. Tominovich, L.V. LaFrance, K.A. Leonard, J.M. Gushue, D.J. Parks, R.R. Calvo, K.L. Milkiewicz, J.J. Marugán, P. Raboisson, M.D. Cummings, B.L. Grasberger, D.L. Johnson, T. Lu, C.J. Molloy, A.C. Maroney, Benzodiazepinedione inhibitors of the Hdm2:p53 complex suppress human tumor cell proliferation in vitro and sensitize tumors to doxorubicin in vivo, *Mol. Cancer Ther.* 5 (1) (2006) 160.
- [30] L. Chen, H. Yin, B. Farooqi, S. Sebt, A.D. Hamilton, J. Chen, p53 alpha-Helix mimetics antagonize p53/MDM2 interaction and activate p53, *Mol. Cancer Ther.* 4 (2005) 1019.
- [31] Y. Lu, Z. Nikolovska-Coleska, X. Fang, W. Gao, S. Shangary, S. Qiu, D. Qin, S. Wang, Discovery of a nanomolar inhibitor of the human murine double minute 2 (MDM2)-p53 interaction through an integrated, virtual database screening strategy, *J. Med. Chem.* 49 (2006) 3759.
- [32] R. Stoll, C. Renner, S. Hansen, S. Palme, C. Klein, A. Belling, W. Zeslawski, M. Kamionka, T. Rehm, P. Mühlhahn, R. Schumacher, F. Hesse, B. Kaluza, W. Voelter, R.A. Engh, T.A. Holak, Chalcone derivatives antagonize interactions between the human oncoprotein MDM2 and p53, *Biochemistry* 40 (2001) 336.
- [33] P.S. Galatin, D.J. Abraham, A nonpeptidic sulfonamide inhibits the p53-mdm2 interaction and activates p53-dependent transcription in mdm2-overexpressing cells, *J. Med. Chem.* 47 (2004) 4163.
- [34] B. Hu, D.M. Gilkes, B. Farooqi, S.M. Sebt, J. Chen, MDMX overexpression prevents P53 activation by the MDM2 inhibitor nutlin, *J. Biol. Chem.* 281 (44) (2006) 33030.
- [35] M. Pazgier, M. Liu, G. Zou, W. Yuan, C. Li, C. Li, J. Li, J. Monbo, D. Zella, S.G. Tarasov, W. Lu, Structural basis for high-affinity peptide inhibition of p53 interactions with MDM2 and MDMX, *Natl. Acad. Sci. U.S.A.* 106 (12) (2009) 4665.
- [36] R.E. Hubbard, *Structure-Based Drug Discovery: An Overview*, first ed., RSC Publishing, Cambridge, 2007, p. 261.
- [37] C.W. Murray, C.A. Baxter, A.D. Frenkel, The sensitivity of the results of molecular docking to induced fit effects: application to thrombin, thermolysin and neuraminidase, *J. Comput. Aided Mol. Des.* 13 (1999) 547.
- [38] A.L. Bowman, Z. Nikolovska-Coleska, H. Zhong, S. Wang, H.A. Carlson, Small molecule inhibitors of the MDM2-p53 interaction discovered by ensemble-based receptor models, *J. Am. Chem. Soc.* 129 (2007) 12809.
- [39] J.H. Lin, A.L. Perryman, J.R. Schames, J.A. McCammon, Computational drug design accommodating receptor flexibility: the relaxed complex scheme, *J. Am. Chem. Soc.* 124 (2002) 5632.
- [40] M. Markowitz, B.Y. Nguyen, F. Gotuzzo, F. Mendo, W. Ratanasuwana, C. Kovacs, J. Zhao, L. Gilde, R. Isaacs, H. Teppeler, Potent antiviral effect of MK-0518, novel HIV-1 integrase inhibitor, as part of combination ART in treatment-naïve HIV-1 infected patients, in: 16th International AIDS Conference, Toronto, Canada, August 13–18, 2006 (no. ThLB0214).
- [41] L.T. Vassilev, B.T. Vu, B. Graves, D. Carvajal, F. Podlaski, Z. Filipovic, N. Kong, U. Kammlott, C. Lukacs, C. Klein, N. Fotouhi, E.A. Liu, In vivo activation of the p53 pathway by small-molecule antagonists of MDM2, *Science* 303 (5659) (2004) 84.
- [42] M.M. Garrett, S.G. David, S.H. Robert, H. Ruth, E.H. William, K.B. Richard, J.S. Arthur, Automated docking using a Lamarckian genetic algorithm and an empirical binding free energy function, *J. Comput. Chem.* 19 (1999) 1639.
- [43] P.A. Kollman, I. Massova, C. Reyes, B. Kuhn, S. Huo, L. Chong, M. Lee, T. Lee, Y. Duan, W. Wang, O. Donini, P. Cieplak, J. Srinivasan, D.A. Case, T.E. Cheatham, Calculating structures and free energies of complex molecules: combining molecular mechanics and continuum model, *Acc. Chem. Res.* 33 (2000) 889.
- [44] L. Kalé, NAMD2: Greater scalability for parallel molecular dynamics, *J. Comput. Phys.* 151 (1999) 283–312.
- [45] V. Hornak, R. Abel, A. Okur, B. Strockbine, A. Roitberg, C. Simmerling, Comparison of multiple Amber force fields and development of improved protein backbone parameters, *Proteins* 65 (2006), 712–765, 725.
- [46] T.J. Dolinsky, P. Czodrowski, H. Li, J.E. Nielsen, J.H. Jensen, G. Klebe, N.A. Baker, PDB2PQR: ep53nding and upgrading automated preparation of biomolecular structures for molecular simulations, *Nucleic Acids Res.* 35 (2007) W522–525.
- [47] D.A. Case, T.E. Cheatham, T. Darden, H. Gohlke, R. Luo, K.M. Merz, A. Onufriev, C. Simmerling, B. Wang, R.J. Woods, The Amber biomolecular simulation programs, *J. Comput. Chem.* 26 (2005) 1668–1688.
- [48] J. Wang, R.M. Wolf, J.W. Caldwell, P.A. Kollman, D.A. Case, Development and testing of a general amber force field, *J. Comput. Chem.* 25 (2004) 1157.
- [49] A. Jakalian, B.J. David, C.I. Bayly, Fast, efficient generation of high-quality atomic charges. AM1-BCC model: II. Parameterization and validation, *J. Comput. Chem.* 23 (2002) 1623.
- [50] L.S. Cheng, R.E. Amaro, D. Xu, W.W. Li, P.W. Arzberger, J.A. McCammon, Ensemble-based virtual screening reveals potential novel antiviral compounds for avian influenza neuraminidase, *J. Med. Chem.* 51 (13) (2008) 3878.
- [51] R.M.A. Knegetel, I.D. Kuntz, C.M. Oshiro, Molecular docking to ensembles of protein structures, *J. Mol. Biol.* 266 (1997) 424.
- [52] J. Shao, S.W. Tanner, N. Thompson, T.E. Cheatham, Clustering molecular dynamics trajectories: 1. Characterizing the performance of different clustering algorithms, *J. Chem. Theor. Comput.* 3 (2007) 2312.
- [53] D.L. Davies, D.W. Bouldin, A cluster separation measure, *IEEE Trans. Pattern Anal. Mach. Intell.* 1 (1979) 224.
- [54] A.E. Garcia, Large-amplitude nonlinear motions in proteins, *Phys. Rev. Lett.* 68 (1992) 2696.
- [55] A. Amadei, A.B. Linssen, H.J. Berendsen, Essential dynamics of proteins, *Proteins* 17 (1993) 412.
- [56] B. Kuhn, P. Gerber, T. Schulz-Gasch, M. Stahl, Validation and use of the MM-PBSA approach for drug discovery, *J. Med. Chem.* 48 (12) (2005) 4040.
- [57] B. Hess, Convergence of sampling in protein simulations, *Phys. Rev. E Stat. Nonlin. Soft Matter Phys.* 65 (2002) 31910.
- [58] [http://dtp.nci.nih.gov/branches/dscb/diversity\\_explanation.html](http://dtp.nci.nih.gov/branches/dscb/diversity_explanation.html). Last checked October 21, 2009.
- [59] <http://zinc.docking.org/vendor0/dbsm/index.html>. Last checked October 21, 2009.
- [60] <http://pubchem.ncbi.nlm.nih.gov/>. Last checked October 21, 2009.
- [61] T.T. Tanimoto, IBM Internal Report, 17 November 1957.
- [62] J. Gasteiger, M. Marsili, Iterative partial equalization of orbital electronegativity: a rapid access to atomic charges, *Tetrahedron* 36 (1980) 3219.
- [63] I. Massova, P.A. Kollman, Computational alanine scanning to probe protein-protein interactions: a novel approach to evaluate binding free energies, *J. Am. Chem. Soc.* 121 (1999) 8133.
- [64] A. Bottger, V. Bottger, C. Garcia-Echeveria, P. Chene, C. Garcia-Echeveria, P. Chene, H.K. Hochkeppel, S.F. Howard, S.M. Picklesley, D.P. Lane, Biochemical characterization of the hdm2-p53 interaction, *J. Mol. Biol.* 269 (1997) 744.
- [65] J.C. Marine, M.A. Dyer, A.G. Jochemsen, MDMX: from bench to bedside, *J. Cell Sci.* 120 (3) (2007) 371.
- [66] H. Yin, G.I. Lee, H.S. Park, G.A. Payne, J.M. Rodriguez, S.M. Sebt, A.D. Hamilton, Terphenyl-based helical mimetics that disrupt the p53/HDM2 interaction, *Angew. Chem. Int. Ed. Engl.* 44 (2005) 2704.
- [67] A.N. Bullock, A.R. Fersht, Rescuing the function of mutant p53, *Nat. Rev. Cancer* 1 (2001) 68.
- [68] T. Fojo, p53 as a therapeutic target: unresolved issues on the road to cancer therapy targeting mutant p53, *Drug Resist. Updat.* 5 (2001) 209.